Quantitative Schlieren imaging based on fringe projection

Pavel Psota[1*], *Marek* Stašík[1], *Jan* Kredba[1], *Vít* Lédl[1], *Darina* Jašíková[1], *Michal* Kotek[1], and *Václav* Kopecký[1]

[1]Faculty of Mechatronics, Informatics and Interdisciplinary Studies, Technical University of Liberec, Studentská 2, 461 17 Liberec 1, Czech Republic

Abstract. An effective yet simple quantitative synthetic Schlieren imaging technique is presented in this paper. A multiplexed fringe pattern displayed on a common laptop screen is observed through a disturbed medium resulting in a change of the fringe pattern. Fourier analysis of such pattern provides high-resolution and almost real time measurement of rays' deflection due to the medium refractive index variation. The developed technique was applied for measurement of a compressible fluid discharge from a narrow channel in a wind tunnel.

1 Introduction

The term "Schlieren" refers to any optical inhomogeneities in a transparent medium and Schlieren photography relies on the the fact that light rays are bent whenever they encounter changes in density of a fluid. Various modifications of Schlieren techniques [1–3] have been used for flow visualization over a hundred year. With the rise of digital sensing technology, Background Oriented Schlieren (BOS) techniques are emerging [4–6]. BOS is an optical flow diagnostic technique used to measure density gradients in a flow field by tracking the apparent distortion of a target dot pattern. The distortion of the dot pattern is typically estimated by cross-correlating an image of the dot pattern without the density gradients (the reference image) with a distorted image viewed through the density gradients (the gradient image). In this paper we propose BOS technique based on fringe projection with spatial carrier frequencies. Such fringe pattern is similar to the pattern obtained by the interference of two tilted plane waves. A Fourier domain analysis allows for accurate yet fast data processing. This approach was applied for measurement of supersonic compressible fluid discharge from a narrow channel in a wind tunnel. The measured density distribution was compared to interferometric results. In addition to the direct use of this technique in various research topics, it can also be used along with interferometry [7] of high-gradient fields in order to subtract mapping error within interferometric data evaluation.

2 Methods

Fig. 1 shows the interaction between a light ray and a schliere. A schliere can be considered as gradient of the index of refraction in a transparent medium. Many experimental arrangements including wind tunnels are designed in order to keep the refractive index along z-axis constant. In Fig. 1 a two-dimensional schliere with a positive gradient of the index of refraction $\partial n/\partial y > 0$ in y-direction is sketched. Before the light ray interacts with the schliere it moves straight and parallel into the z-direction.

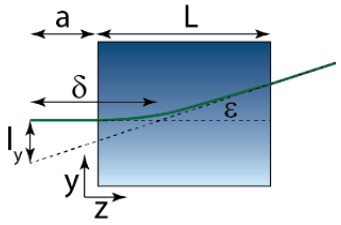

Fig. 1. Geometry of light refraction of a 2D schliere with a gradient in y-direction.

When the ray travels within the schliere it is bent towards the regions of higher index of refraction with a curvature

$$\frac{\partial^2 y}{\partial^2 z} = \frac{1}{n_0}\frac{\partial n}{\partial y} \quad (1)$$

and after travelling a distance of L it is bend by the angular ray deflection ε_y

$$\varepsilon_y = \frac{L}{n_0}\frac{\partial n}{\partial y}. \quad (2)$$

When observed through the schliere, the banded ray seems to be shifted about

$$l_y \approx \delta\varepsilon_y = \frac{L\delta}{n_0}\frac{\partial n}{\partial y}, \quad (3)$$

where $\delta = a + L/2$.

For simplification, let's keep the one-dimensional case (omitting $\partial n/\partial x$). We will expand the description in both dimensions x, y later in the text. Let us assume that a fringe pattern with spatial carrier frequency k_{y0} :

$$I(y) = A + \cos(k_{y0}y) \quad (4)$$

is located on the back side of an experimental section, see Fig. 2a. When observing the fringe pattern through an area

* Corresponding author: pavel.psota@tul.cz

with the presence of flow, the observed fringe pattern is modified due to the schliere effect as:

$$I(y) = \mathrm{A} + \cos\left(k_{y0}y + \varphi_y(y)\right) \qquad (5)$$

where $\varphi_y(y) = k_{y0}l_y(y)$ is phase due to the ray deflection l_y in y-direction, see the green ray in Fig. 2a. It is obvious that the phase φ_y is the key to retrieve the ray deflection. Rewriting (5) using complex exponential yields in

$$I(y) = A + 1/2\,C(y) + 1/2\,C^*(y), \qquad (6)$$

where $C(x,y) = \exp\left[i\left(\varphi_y(y) + k_{y0}y\right)\right]$. Equation (6) in Fourier domain:

$$\hat{I}(k_y) = \hat{A} + \hat{C}(k_y - k_{y0}) + \hat{C}^*(k_y + k_{y0}) \qquad (7)$$

(with the spatial frequency coordinates k_y) is composed of a central DC term - $\hat{A}$ and two conjugated components $\hat{C}$, $\hat{C}^*$ located symmetrically from the center of the spectrum, see Fig. 2b. The roof symbol ˆ denotes Fourier spectrum and the superscript * denotes complex conjugation. The introduced spatial carrier frequency k_{y0} plays a key role in the clear separation of all spectral components $\hat{A}$, $\hat{C}$, $\hat{C}^*$in the Fourier Domain and must be sufficiently high to avoid any mutual overlap of the components. On the other hand, k_{y0} cannot be too high in order to meet the Nyquist criterion (resolve the cosine pattern by the camera sensor).

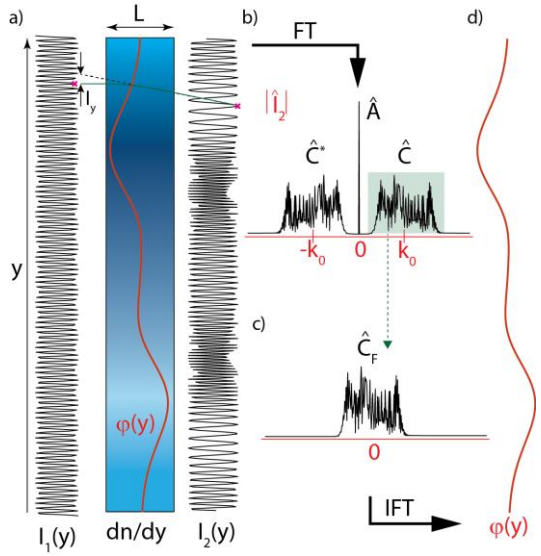

Fig. 2. Principle of the fringe projection technique in 1D (along y-axis): a) fringe pattern before I1 and after I2 propagation through the nonhomogeneous media; b) the Fourier amplitude spectrum of the fringe patter; c) the Fourier amplitude spectrum after a band-pass filtering and shifting; d) phase distribution retrieved from filtered complex field.

Once the spectral components are separated, it is possible to filter out the desired spectral component $\hat{C}$ (containing the phase φ) using bandpass filter around the carrier spatial frequency k_{y0} (see the green interval in Fig. 2b). Considering the shift property of the Fourier Transform, the filtered spectrum $\hat{C}_F$ (subscript F denotes filtered spectrum without $\hat{A}$ and $\hat{C}^*$) can be shifted about the spatial frequency in order to remove the linear phase carrier, see Fig2c. The filtered and shifted spectrum $\hat{C}_F$ isn't any longer Hermitean so its inverse Fourier Transform will contain non-zero both real and imaginary parts and hence the phase (see Fig. 2d) can be retrieved as:

$$\varphi_y(y) = arctan\left(\frac{Im\{C_F(y)\}}{Re\{C_F(y)\}}\right). \qquad (8)$$

The spatial frequency k_{y0} as seen by a camera depends on magnification of imaging system and/or may not be accurately know. Moreover, some optical aberrations without the presence of a phenomena due to e.g. optical windows may be introduced. Therefore, a double shot measurement is recommended. Let us assume a measurement at the steady/reference state without presence of a phenomenon resulting in C_{F0} and another measurement performed with the presence of the phenomenon that is processed in the very same way to get C_{F1}. The measurement with the phenomenon can be related to the reference state measurement as

$$\varphi_y(y) = arctan\left(\frac{Im\{C_{F1}(y)C^*_{F0}(y)\}}{Re\{C_{F1}(y)C^*_{F0}(y)\}}\right). \qquad (9)$$

It is important to note that phase φ_y is wrapped within 2π interval and thus, if the phase range exceeded, a spatial unwrapping algorithm [8] must be applied. A displacement l_y of the fringe at each pixel in y-direction can be obtained from the phase φ_y as

$$l_y(y) = \varphi_y(y)/k_{y0}. \qquad (10)$$

Assuming geometry in Fig. 1 and (3), the displacement can be used to calculate refractive index slope

$$\frac{dn}{dy} = arctan\left(\frac{l_y(y)}{\delta}\right)\frac{n_0}{L}. \qquad (11)$$

As x and y coordinates are orthogonal, the same analysis can be done for x-direction. However, due to dynamic behavior of flow, it is not possible to measure $\frac{dn}{dy}$ and $\frac{dn}{dx}$ one after the other. The solution is a using of the multiplexed fringe pattern resulting in the observed pattern

$$I(x,y) = \mathrm{A} + \cos\left(k_{y0}y + \varphi_y(x,y)\right) + \cos\left(k_{x0}x + \varphi_x(x,y)\right) \qquad (12)$$

that is modified by phases φ_x, φ_y due to deflections l_x, l_y in both orthogonal directions. Such fringe pattern is processed independently for each direction and hence the displacements l_x, l_y, eventually refractive index slope maps $\frac{dn}{dx}$, $\frac{dn}{dy}$ can be computed.

3 Measurement of flow discharge

The experimental arrangement is shown in Fig. 3. It is a very simple configuration consisting of an image of the fringe pattern (FP) displayed on a laptop screen, the measured area (MA) and Phototron FASTCAM Mini WX100 high-speed camera with a 70mm focal length

lens. The camera resolution is 2048×2048 pixels, each having extension of 20μm.

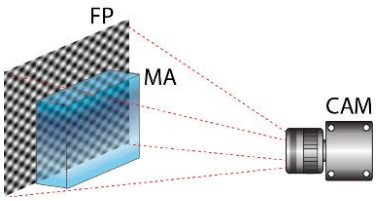

Fig. 3. Experimental arrangement of the fringe projection technique: FP – fringe pattern, MA – measured area (volume), CAM – camera with a lens.

This technique can however be used with any imaging system providing sufficient field of view, spatial and temporal resolution for the particular phenomenon under investigation. In our case, the phenomenon under investigation was a supersonic compressible fluid discharge from a narrow channel in a wind tunnel. The narrow channel was formed by two parallel walls and behind the channel there was a settling chamber, see Fig. 4. The test section had optical windows on both side for the flow and the fringe pattern observation.

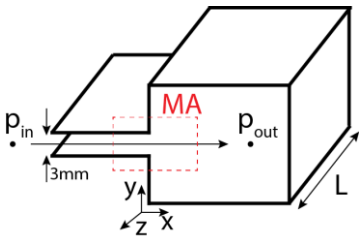

Fig. 4. Basic concept of the narrow channel and the settling chamber measurement. Dashed rectangle represents the investigated area.

During measurement, air flows through the channel due to pressure gradient. Air enters the test section at ambient conditions thus total pressure P_{in}=98.05kPa was equal to the barometric pressure. Static pressure at the outlet of the narrow channel P_{out}=23.87kPa in the settling chamber was also measured for further quantitative evaluation. The intensity fringe pattern was composed of a multiplexed orthogonal cosine fringe patterns with carrier frequencies in *x', y'* directions. The x', y' coordinate system was rotated around 45° to a global reference frame (*x, y*) defined by the narrow channel axis, see Fig 5a.

The fringe pattern was observed through optical glasses on the wind channel walls. The fringe pattern was firstly captured at reference state (P_{in}=P_{out}=98.05kPa) yielding in pattern denoted as I_R. Then the observed intensity fringe pattern was modified due to the presence of the air flow (P_{in}≠P_{out}). The modified fringe pattern I_M was also captured. The both fringe patterns were processed in Fourier domain, see Fig. 5b and phase maps P_1 and P_2 were retrieved using the procedure described above, see Fig. 5c. The phase maps P_1 and P_2 are related to displacements in direction of spatial frequency k-vectors $\boldsymbol{k_1} = (\boldsymbol{k_{x1}}, \boldsymbol{k_{y1}})$, $\boldsymbol{k_2} = (\boldsymbol{k_{x2}}, \boldsymbol{k_{y2}})$, see Fig. 5b.

Magnitudes of the spatial frequencies vectors $|\boldsymbol{k_1}| = |\boldsymbol{k_2}| = 0.45 mm^{-1}$ can also be obtained from the Fourier spectrum. Finally, displacements l_1, l_2 and refractive index slopes $\frac{dn}{dx'}, \frac{dn}{dy'}$ can be computed using (10) and (11).

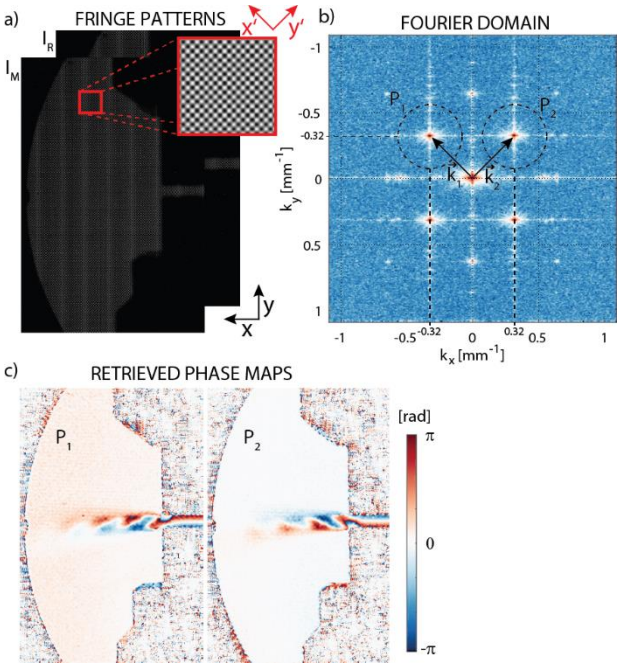

Fig. 5. Data processing: a) observed fringe pattern before IR and after IM the flow was presented; b) the amplitude Fourier spectrum with carrier frequencies; c) retrieved phase maps that proportional to fringe displacement in x', y' direction, respectively.

Usually, refractive index slopes along parallel and perpendicular direction (*x*, *y* – reference frame) to the channel axis are of the main concern. The reference frame of the fringe pattern (*x'*, *y'*) was therefore rotated about $\theta = 45°$ in order to retrieve slope maps:

$$\begin{pmatrix} \frac{dn}{dx} \\ \frac{dn}{dy} \end{pmatrix} = \begin{pmatrix} cos\theta & -sin\theta \\ sin\theta & cos\theta \end{pmatrix} \begin{pmatrix} \frac{dn}{dx'} \\ \frac{dn}{dy'} \end{pmatrix}. \qquad (13)$$

The slope maps are shown in Fig. 6 (left column). In order to verify the approach, an interferometric measurement in the same flow regime was realized.

It is important to note that the interferometric arrangement had very different imaging system from the fringe projection measurement yielding in different spatial resolution. In addition, both measurements (albeit with the same controllable parameters) were performed at different times. Therefore, fringe projection and interferometric results are not directly comparable. However, qualitative comparison of the fringe projection method (left column) and interferometric measurement (right column) evinces a high degree of agreement. Unlike deflection (Schlieren) techniques, interferometers measure the refractive index (not just ray deflection due the refractive index gradient) and thus maps in Fig. 6 (right column) were obtained as slope of interferometrically measured refractive index.

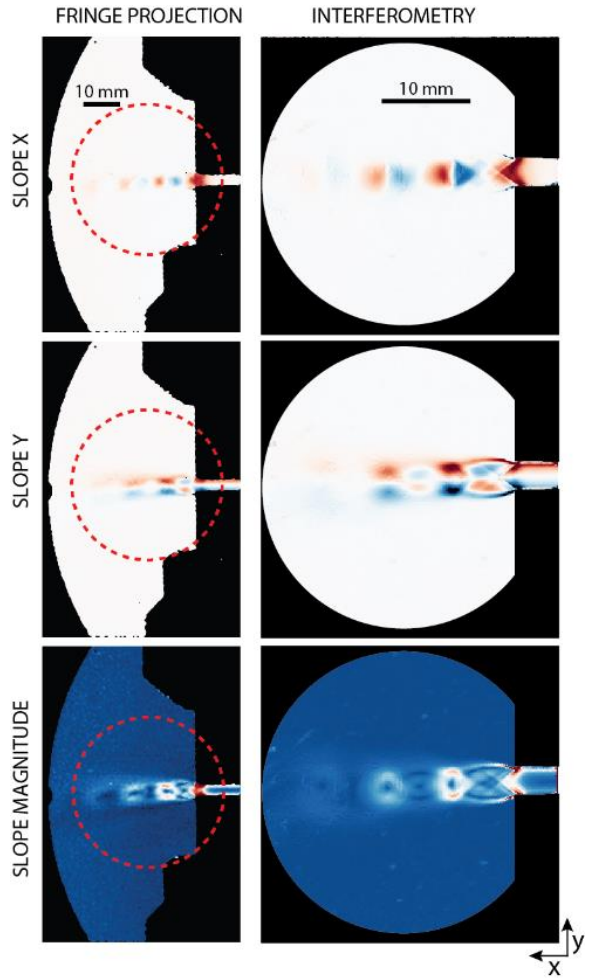

Fig. 6. Slope maps dn/dx, dn/dy and the magnitude of the gradient vector measured by the fringe projection technique and by interferometry. The red dashed circle indicates interferometer's field of view.

In the opposite approach, we obtained the density distribution (see Fig. 7) by numerical integration of slope maps in Fig. 6 measured by the fringe projection technique and using the Gladstone-Dale equation:

$$\rho(x,y) = \frac{p_{out}}{RT_0} + \frac{\Delta n(x,y)}{K}. \qquad (14)$$

In (14), K=0.00022m^3/kg represents the Gladstone-Dale constant, T_0=296K denotes the ambient air temperature, R=287.1 J/(kg·K) is the specific gas constant and $\Delta n(x,y)$ is the refracitve index change map resulted from the numerical integration.

The numerical integration is sensitive to local outliers and therefore there are some erroneous areas close to edges/walls in the image.

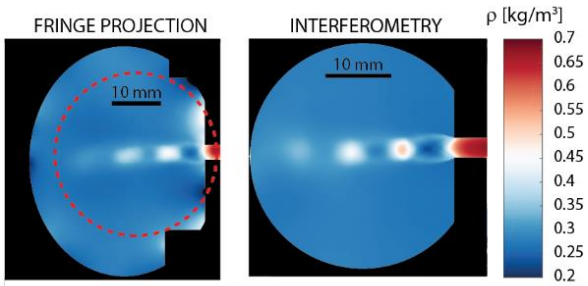

Fig. 7. Density distribution computed from slope maps measured by the fringe projection (left), and density distribution measured directly by interferometry (right).

4 Conclusion

This paper presents a very effective technique for characterization of fluid flow. The technique based on fringe projection is sensitive to ray deflection caused by gradient of the index of refraction in a transparent medium. A well-defined multiplexed cosine fringe pattern is observed through a measured area and modification of the pattern indicates the refractive index variation caused by a phenomenon. The displacement of the fringe pattern in orthogonal directions can be evaluated in each pixel using Fourier analysis. Assuming parameters of the experimental arrangement, the displacement can further be used for quantitative analysis of various phenomena. The developed fringe projection technique was successfully applied for the research of a fluid flow in a narrow channel including a free jet at the channel exit. The experimental section was built in a wind tunnel allowing for a high pressure difference and thus high flow velocity through the channel. The wind tunnel experiment construction assures mostly constant refractive index along the optical axis and thus quantitative analysis was performed. The results were compared to results obtained by interferometer with a good agreement. In the future, this approach will also be used along with interferometry of high-gradient fields in order to subtract mapping error and refine interferometric measurements.

Acknowledgments

We gratefully acknowledge the support of the Grant Program of the Technical University of Liberec (project number PURE-2020-3010). We thank the people from the Aerodynamics Laboratory in NovýKnín (part of The Institute of Thermomechanics of the Academy of Sciences of the Czech Republic) for their help and discussion in setting up experiments in the wind tunnel.

List of symbols

x, y, z [m]	Cartesian coordinate system
n [1]	Refractive index
L [m]	Length of the measured area
l_y [m]	Ray shift
ε [rad]	Angle of deflection
$I, \hat{I}$ [1]	Intensity and its Fourier image
$A, \hat{A}$ [1]	Mean intensity (DC term) and its term in Fourier domain
k [m^{-1}]	Wavenumber
$\boldsymbol{k}$ [m^{-1}]	wavevector
φ [rad]	Optical phase
θ [rad]	Angle of rotation
P_{in} [Pa]	Total pressure
P_{out} [Pa]	Outlet pressure
ρ [$kg \cdot m^{-3}$]	Density
T_0 [K]	Temperature
K [m^3/kg]	Gladstone-Dale constant
R [$kg \cdot K$]	specific gas constant
$\hat{X}$	Fourier spectrum of X
X^*	Complex conjugation of X

References

1. W. Merzkirch., *Handbook of Experimental Fluid Mechanics* (Springer, Berlin, Heidelberg, 2007)
2. G. S. Settles, and M. J. Hargather , Measurement Science and Technology, **28** (2017)
3. A. Eder, and M. Jordan, *Techniques and Applications* (Springer, Berlin, Heidelberg, 2001).
4. S. B. Dalziel, G. O. Hughes and B.R. Sutherland, Experiments in Fluids, **28** (2000)
5. H. Richard, and M. Raffel, Measurement Science and Technology **12**, (2001)
6. J. A. Letelier, P, Herrera, N. Mujica, and J.H. Ortega, Exp Fluids **57**, 18 (2016)
7. P. Psota, P. Dančová, G. Cubreli, V. Lédl, T. Vít, R. Doleček, and O. Matoušek, International Journal of Thermal Sciences **145**, 106029 (2019)
8. R. M. Goldstein, H. A. Zebker, and C. L. Werner, Radio Science **23**, (1988)